Biomimetic Porous MXene Sediment-Based Hydrogel for High-Performance and Multifunctional Electromagnetic Interference Shielding

Journal:	*ACS Nano*
Manuscript ID	nn-2022-06164n.R3
Manuscript Type:	Article
Date Submitted by the Author:	16-Aug-2022
Complete List of Authors:	Yang, Yunfei; Shandong University Wu, Na; ETH Zürich, Li, Bin; Shandong University Liu, Wei; Shandong University, Institute of Crystal Materials Pan, Fei; University of Basel zeng, zhihui; Shandong University, Material Science and Engineering Liu, Jiurong; Shandong University School of Control Science and Engineering,

Biomimetic Porous MXene Sediment-Based Hydrogel for High-Performance and Multifunctional Electromagnetic Interference Shielding

Yunfei Yang,[a] Na Wu,*[,b] Bin Li,[a] Wei Liu,[c, d] Fei Pan,[e] Zhihui Zeng,*[, a] and Jiurong Liu*[, a]

[a] Key Laboratory for Liquid-Solid Structural Evolution and Processing of Materials, School of Materials Science and Engineering, Shandong University, Jinan, Shandong, 250061, China.

[b] Department of Chemistry and Applied Biosciences, ETH Zurich, CH-8093 Zurich, Switzerland.

[c] State Key Laboratory of Crystal Materials, Institute of Crystal Materials, Shandong University, Shandong, 250100, China.

[d] Shenzhen research institute of Shandong University, Shenzhen, 518052, China.

[e] Department of Chemistry, University of Basel, Mattenstrasse 24a, BPR 1096, CH-4000 Basel, Switzerland.

*Corresponding author:

E-mail: na.wu@org.chem.ethz.ch; zhihui.zeng@sdu.edu.cn; jrliu@sdu.edu.cn

Abstract: Developing high-performance and functional hydrogels that mimick biological materials in nature is promising yet remains highly challenging. Through a facile, scalable unidirectional freezing followed by salting-out approach, a type of hydrogels composed of "trashed" MXene sediment (MS) and biomimetic pores are manufactured. By integrating the honeycomb-like ordered porous structure, highly conductive MS, and water, the electromagnetic interference (EMI) shielding effectiveness is up to 90 dB in the X band and can reach more than 40 dB in the ultra-broadband gigahertz band (8.2–40 GHz) for the highly flexible hydrogel, outperforming previously reported porous EMI shields. Moreover, thanks to the stable framework of the MS-based hydrogel, the influences of water on shielding performance are quantitatively identified. Furthermore, the extremely low content of silver nanowire is embedded into the biomimetic hydrogels, leading to the significantly improved multiple reflection-induced microwave loss and thus EMI shielding performance. Last, the MS-based hydrogels allow sensitive and reliable detection of human motions and smart coding. This work thus not only achieves the control of EMI shielding performance *via* the interior porous structure of hydrogels, but also demonstrates a waste-free, low-cost, and scalable strategy to prepare multifunctional, high-performance MS-based biomimetic hydrogels.

Keywords: hydrogel, biomimetic, multifunctional, electromagnetic interference, MXene sediment

Introduction

The advancement of gigahertz (GHz) band communication technologies has significantly brought convenience for humans while it also leads to hazardous electromagnetic interference (EMI) or radiation.[1-4] To this end, high-performance, easy-manufacturing, adjustable-performance, and low-cost EMI shields are urgently desired.[5, 6] Since introducing the micrometer-sized pores in EMI shields can facilitate multiple reflections of incident electromagnetic waves (EMWs) and effectively improve the EMI shielding effectiveness (SE), recently cellular foams/aerogels have attracted more and more attention for preparing high-performance EMI shields.[7-10] However, compared with the bulk shields, the foams/aerogels-based shields generally suffer from fragility as well as poor flexibility.[11] This limits the development of high-performance EMI shields demanding good mechanical toughness, flexibility, and even stretchability, which are especially desired for next-generation flexible devices. The hydrogels, composed of a cellular structure filled with plenty of water and a network of crosslinking hydrophilic building blocks, can reveal satisfactory mechanical flexibility, elasticity, toughness, fatigue resistance, and especially stretchability.[12-15] Moreover, abundant water-enriched pores are promising for increasing the multiple reflections of incident EMWs and enhancing the polarization loss capability derived from water molecular and hydrogen-bond networks.[16-18] This promises the hydrogels acting as high-performance EMI shielding architectures.

Generally, designing a highly crosslinked polymer framework to sustain the hydrogel without collapse and integrating the conductive nanomaterials into the hydrogel to increase the dissipation of incident EMWs are essential for obtaining high-performance hydrogel-based EMI shields. Thanks to the high conductivity, excellent mechanical properties, and large aspect ratio, the

nanomaterials such as carbon nanotube (CNT), graphene, or transition metal carbide and/or nitride (MXene) are most popularly employed for improving the mechanical, electrical, and EMI shielding performance of hydrogels.[19, 20] For instances, the poly(acrylic acid)/chitosan/amorphous calcium carbonate hydrogels embedded with 4.76 wt% reduced graphene oxide (rGO) and 4.76 wt% CNTs were prepared, respectively, showing an X-band (8.2–12.4 GHz) EMI SE of 48 dB at a thickness of 3 mm and an X-band SE of ~60 dB at 9 mm thickness, respectively.[21] Liu *et al.* fabricated the 4 wt% Ti_3C_2-MXene-functionalized poly(3,4-ethylenedioxythiophene) polystyrene sulfonate (PEDOT: PSS) hydrogels, showing an X-band EMI SE of 51.7 dB.[22] Here, a high fraction of polymer has to be employed to crosslink the inorganic conductive nanomaterials for preparing robust hydrogels due to the weak interfacial interactions between the nanomaterials, moreover, the challenge in well dispersing these conductive nanomaterials with a high fraction in the polymer matrices exists for the reported hydrogels.[23] However, regarding the hydrogel-based EMI shields, too high content of insulting polymer is not beneficial for fully utilizing the conductivity and EMI shielding properties of the functional nanomaterials.[24] Moreover, since the mechanical strength of the cell walls is not satisfactory at too high polymer contents, designing cellular morphology such as biomimetic ordered micrometer-sized pores, which has been proven to be efficient to improve the EMI shielding performance, remains highly challenging for the hydrogel-based EMI shields.[7, 25-27] Developing robust hydrogels with fewer polymers and more controllable cellular morphologies are highly demanded to advance the development and understanding of the structure-performance relationships of hydrogel-based EMI shields. Last but not the least, the preparation or processing of these often-employed conductive nanomaterials including CNTs, graphene, and MXene layers for preparing the EMI shielding hydrogels still suffers from high cost, low yields, or additional functionalization

treatments, thereby limiting the practical application requiring cost and environmental efficiency. We notice that the MXene sediment (MS), consisting of unetched MAX and unexfoliated multilayered MXene (m-MXene) as well as a tiny amount of residual single/few-layered MXene, is generally trashed away during preparing the MXene layers that have been widely developed in supercapacitors, biomedicine, and sensors.[28-30] This surges the constructing cost of burgeoning MXene-based devices and wastes quite some amount of materials. Interestingly, we have ascertained that the "trashed" MS shows high electrical conductivity, high yield, and high concentration in water, which are highly anticipated for preparing high-performance EMI shields or hydrogel-based devices.

Here, through a facile, scalable unidirectional freezing and subsequent salting-out approach, we successfully employed a small amount of polyvinyl alcohol (PVA) to crosslink the MS for preparing a type of robust, highly conductive hydrogels with unidirectional, micrometer-sized honeycomb-like pores. The high-toughness cell walls, derived from the synergy of PVA and MS, not only stabilized the biomimetic ordered pore structure but also contributed to the high mechanical flexibility and stretchability of the MS-based hydrogels. The synergistic interactions of pores, MS-based conductive network, and considerable interfaces between MS and PVA, rendered the hydrogels with high EMI shielding performance. Our MS-based hydrogels exhibited the X-band EMI SE of 31 to 91 dB at a thickness of 1.0 to 7.5 mm, respectively, and the SE of the 2.0 mm-thick hydrogels was more than 40 dB over the ultra-broadband GHz frequency range, involving X-band, Ku-band (12.4–18 GHz), K-band (18–26.5 GHz), and Ka-band (26.5–40 GHz). This performance was on par with that of the best EMI shielding materials ever reported. Moreover, we quantitatively identified the influences of water on EMI shielding performance *via* a facile, resumable control of the water fraction in the hydrogel, advancing a valuable understanding of the superiority of hydrogel

for EMI shielding monoliths. Furthermore, the extremely low content of silver nanowire (AgNW) was easily embedded into the MS-based biomimetic hydrogel, significantly enhancing the EMI shielding performance. With a mere 0.16 wt% AgNW, the EMI SE of the hydrogels drastically increased from 44 to 66 dB when the propagation direction of the incident EMWs was perpendicular to the aligned pore channels. In addition, the mechanical ultra-flexibility of the conductive MS-based hydrogels contributed to the implementation of high-performance human motion detections as wearable sensors. The multifunctional MS-based hydrogels thus possess high application potentials for next-generation electronics.

Results and discussion

The fabrication processes of MS-based hydrogels are exhibited in **Figure 1**a, which comprises the delamination of Ti_3AlC_2 MAX, directional freezing, and salting-out approach. Through minimally intensive layer delamination on rocklike Ti_3AlC_2 MAX (Figure S1),[25] the supernatant with high-quality single/few-layered $Ti_3C_2T_x$ MXene nanosheets (supernatant) was separated (Figure S2), and the sediment composed of unetched MAX phase and un-exfoliated m-MXene as well as a tiny amount of MXene layers was left. Generally, the sediment was typically discarded, which resulted in the waste of materials and surges in MXene synthesis costs.[31-33] To avoid this, after decanting the supernatant, the sediment was redispersed in the water to form homogeneous MS aqueous dispersion with an extremely high solid content that MXene dispersion cannot reach. This is reflected by the vicious feature and stability of MS (Figure 1b). The components of MS have presented in the X-ray diffraction (XRD) patterns in Figure S3. The typical diffraction peaks of $Ti_3C_2T_x$ MXene and Ti_3AlC_2 MAX could be indexed in the patterns of MS, illustrating the presence

of unetched MAX phase and un-exfoliated m-MXene.[34-36] Scanning electron microscope (SEM) images and energy dispersive spectroscopy (EDS) mappings are also applied to record the existence of the phase components in MS (Figure 1c and Figure S4). As shown in the transmission electron microscope (TEM) images (Figure 1d and e, and Figure S5), the coexistence of MAX phase, m-MXene, and MXene layers is further verified in MS, which is consistent with the analysis in XRD and SEM.

In consideration of weak interactions between MS particles that cannot form the freestanding architecture, the PVA is utilized as an adhesive to construct the MS-based hydrogel. In the meanwhile, such "trashed" MS particles interconnect to efficiently improve the conductivity of hydrogel as well, which is vital for high-performance EMI shielding. Specifically, by pouring the MS/PVA suspensions into a Teflon mold with a metallic bottom immersed in liquid nitrogen, the ice crystals grew and elongated along the temperature gradient, extruding the MS and PVA to form a composite framework.[37] More importantly, benefiting from this extrusion, a higher solid concentration and a closer packing of PVA chains and MS were obtained for the subsequent salting-out approach.[12] After immersing the freezing gel in a kosmotropic salt solution, the preconcentrated PVA chains, and MS further strongly coalesced to form the crosslinked, high-strength cell walls, which were stabilized by multiple intermolecular hydrogen-bonding and hydrophobic interactions.[14, 38, 39] In Figure 1f, the ordered and aligned micrometer-sized pore channels of MS/PVA hydrogels are exhibited in the through-plane direction that is parallel to the growth direction of ice crystals, compared with the random pores in the in-plane direction (Figure S6). The MS is uniformly distributed in the hydrogels as verified by the EDS mappings (Figure 1g). Profiting from the low-cost MS and the facile, scalable preparation approach, the large-area MS-based hydrogel with

dimensions of 21 × 30 cm^2 (larger than the A4 paper) is prepared (Figure 1h). The hydrogel can also support a person weighing 65 kg without any damage (Figure 1h), showing the good mechanical toughness and stability. In addition, the MS-based hydrogels also exhibit good mechanical flexibility including bending, twisting, and even stretching (Figure 1i), outperforming that of the typical cellular foams/aerogels. The MS-based hydrogel holds up a load more than 200 times heavier than itself, further showing the high toughness.

To further analyze the mechanical properties, the tensile stress-strain curves are shown in Figure 1j. With increasing PVA content, the applied stress on hydrogels can be transferred from rigid MS particles to the surrounding soft polymers, resulting in the increased fracture strain of hydrogels. However, a higher MS content or a lower PVA content of hydrogel has higher tensile strength and modulus due to the high modulus of inorganic MS as well as the generated strong interfaces between MS and PVA (Figure 1j and k). The MS-based hydrogels with a small fraction of polymer such as 20 wt% PVA show the highest tensile strength and modulus. It is also easy to understand that a too less polymer content such as 10 wt% PVA is not beneficial for achieving high mechanical properties (inset in Figure 1j), further implying the weak interfacial interactions between MS particles and the importance of the introduction of a small fraction PVA. In order to reveal the mechanical properties of hydrogels with material consumption, the M_C, defined as the ratio of modulus to the solid content of hydrogels, is calculated. Compared with the hydrogels ever reported (Figure 1l and Table S1), the MS-based hydrogels with 20 wt% PVA possess a higher M_C, showing the superior mechanical property of the MS-based hydrogels even at a low material consumption. Therefore, the aligned cell walls are robust and hardly collapsed, leading to the successful implementation of the biomimetic ordered pore microstructure. Considering the effects of aligned

pore structure on mechanical strength, the mechanical tests are carried out in both parallel and perpendicular directions concerning pore channel directions, as exhibited in Figure S7. The parallel tensile strength and modulus are ~140 and ~248 kPa, respectively, higher than those in the perpendicular direction with ~101 and 120 kPa, respectively. In short, thanks to the rational design of building blocks, MS-based hydrogels showed promising mechanical performance.

Increasing PVA or decreasing MS content is against the formation of the conductive network in the hydrogel, leading to the declined conductivity from 1.6 to 0.2 S/m (Figure 1m). Similarly, as shown in **Figure 2**a, the increased PVA content results in the declined EMI SE. The average X-band SE value of 44.7 dB, signifying that more than 99.997% of incident EMWs are blocked, is obtained for the 2 mm-thick MS-based hydrogels with 20 wt% PVA. With increasing PVA content to 80 wt%, the average SE of hydrogels dramatically reduces to 22.2 dB, which still surpasses the commercial SE requirement of 20 dB.[40-42] Compared with a SE of ~0.4 dB of freeze-dried PVA aerogel (Figure S8a), the EMI SE of pure PVA hydrogel is ~17 dB, demonstrating the role of the interior water plays in improving the EMI SE. It is also observed that the theoretically calculated SE of the DI water is displayed from 8.8 to 15.6 dB in the X band, which is slightly lower than the tested SE value of the pure PVA hydrogels (Figure S8b). This can be attributed to the multiple reflection capability derived from the internal porous structure.[30, 43] Despite the powerful capability of water for dissipating EMWs, the pure PVA hydrogel cannot achieve a satisfactory SE value due to the lack of a conductive component. This indicates the necessity of MS in the composite hydrogels for high EMI shielding performance.

In general, EMI shielding performance is influenced by the reflection, absorption, and multiple reflections, corresponding to the mobile charge carriers, electric dipoles, and interior

interfaces/surfaces, respectively.[44] To clarify the EMI shielding mechanism of hydrogels, the total SE (SE_T), and shielding by reflection (SE_R) and absorption (SE_A) are exhibited (Figure 2b). Here, the SE_A dominated SE_T of the hydrogels, which is similar to that of other porous foams/aerogels ever reported.[45, 46] The increased PVA fraction leads to the decreased mobile charge carriers, and thus the SE_R is decreased. Furthermore, the declined MS content impairs the interfacial polarization and dipole polarization of surface functional groups on MS. These dramatically decrease the SE_A and thus SE_T of MS-based hydrogels with increased PVA contents. The transmission (*T*), absorption (*A*), and reflection (*R*) power coefficients of MS-based hydrogels are utilized to further reveal the shielding process, as shown in Figure 2c. The *R* values mainly depend on the difference in impedance between two sides of the incident interface. Thus, the decreased conductivity stemming from increased PVA content improves the impedance matching between hydrogel and air, inducing the declined *R*. Since the reflection behavior arises before absorption, the variation tendency of *A* is opposite. Most (62%–85%) of incident EMWs are firstly reflected because of the mismatched impedance at the hydrogel/air interface, and a fraction of EMWs (15%–37%) penetrates the hydrogel and are dissipated by the cell walls and water. For the pure PVA hydrogel, the *R* is also higher than *A* because the permittivity of water causes the mismatched impendence (Figure S8c). Here, the micrometer-sized pore-induced multiple reflections of incident EMWs can lead to increased interactions between the EMWs and the cell walls.[7, 10, 25, 26] Thus, the hydrogels have a high SE and a low transmission ($T<10^{-4}$). In a word, the synergistic interactions of the MS, PVA, water, and pore structure in the hydrogels contribute to the high EMI shielding performance.

Adjusting the thickness of MS-based hydrogels is an efficient approach to control the EMI SE. As shown in Figure 2d, with increased thickness of hydrogels from 1.0 to 7.5 mm, the EMI SE lifts

from 31 to 91 dB. The thicker hydrogel conduces to more interactions between EMWs and cell walls, exhibiting higher SE_A and SE_T (Figure 2e). At a thickness of 7.5 mm, the EMI SE can reach up to 91 dB, surpassing that of most porous architectures and showing great potential in EMI shielding applications. Furthermore, the solid content directly affects the EMI shielding performance.[47] By altering the addition of DI water in MS/PVA precursor dispersion, a series of MS-based hydrogels with various solid contents (12.5 wt%–21 wt%) were constructed. As the solid content increases, the EMI SE values lift from 31 to 49 dB, achieving a significant improvement (Figure 2f). The quantitative and wide-range controllability of the EMI SE is thus achieved by controlling the thickness and solid content of the hydrogels. To exhibit superior shielding performance, the SE divided by sample thickness (SE/*d*) values of hydrogels-based shields and typical aerogel/foam-based shields are summarized in Table S2. The performance of our hydrogel-based EMI shields is comparable to that among the best shielding materials ever reported. More importantly, the functional MS embedded into hydrogels has an immense superiority in easily controlling the concentration with a wide range of 20–90 wt% in total solid, which is hardly rivaled by other conductive nanomaterials (Table S1). This leads to extremely wide-range controllability of MS contents in our MS-based hydrogels and thus EMI SE values. In other words, only a small fraction of insulating polymers, easily deteriorating the utilization of intrinsic conductivity of MS, is enough for preparing the robust, functional MS-based hydrogels, which outperforms that of the other hydrogels ever reported.

Thanks to the high mechanical flexibility and stability, the MS-based hydrogels demonstrate good EMI shielding stability and reliability even after the 1000-cycle bending treatments (Figure 2g and Figure S9a). This shows the potential of MS-based hydrogels in the wearable application. With

the iterative upgrading of communications technologies, the working frequency of electrical devices shifts to a higher GHz frequency range. The EMI SE of MS-based hydrogels is higher than 40 dB (Figure 2h) in the typical GHz frequency range including X band, Ku band (12.4–18 GHz), K band (18–26.5 GHz), and Ka band (26.5–40 GHz), further verifying the high, GHz broadband shielding performance and high application potential.

Apart from the mechanical ultra-flexibility, another immense superiority of the hydrogel-based EMI shields that the cellular aerogel/foams cannot rival is the potent polarization loss capability derived from the water filled in the pores.[16, 48] Nevertheless, this critical factor has been barely explored and never quantified in detail. Herein, an *in-situ* and reversible control of the water fraction of MS-based hydrogels is achieved, when the pore structure and macrostructure of hydrogels can be maintained due to the good mechanical properties of the MS-based cell walls (**Figure 3**a). With decreasing water content, the EMI SE exhibits an obvious decline from 44 to 14 dB, corresponding to the values of the original MS-based hydrogels and aerogels without water, respectively (Figure 3b, c). Furthermore, because of the strong crosslinking and hydrophilia of building blocks, the water fraction can be recuperated after the freeze-dried MS-based hydrogel (MS/PVA aerogel) is immersed in DI water. The EMI shielding performance (SE_T, SE_A, and SE_R) of recuperative hydrogels accordingly return. This quantitatively shows the contribution of the water to the EMI shielding performance of the hydrogels. Moreover, we can conclude that owing to the plentiful water incorporated into the porous hydrogels, the EMI SE greatly outperforms that of the corresponding cellular foams/aerogels with the same building framework. This reveals the huge advantages of hydrogels in preparing high-performance EMI shields. It is also worthy to note that the mechanical flexibility and stretchability can return well for the MS-based hydrogel transforming from the

corresponding aerogel, implying the good mechanical strength and stability of the MS-based scaffolds in hydrogels (Figure S9b). This reversibility between our MS-based hydrogel and aerogel also assures the storage stability of our hydrogels in practical applications. In short, a quantified evaluation of the influences of water on EMI shielding performance for the hydrogels is efficiently achieved, achieving the designation of high-performance EMI shielding hydrogels.

AgNW with a large aspect ratio are employed to improve the conductivity of cell walls (Figure S10), further improving the EMI shielding performance of the MS-based hydrogels. [46] Interestingly, with a tiny addition of 0.16 wt% (the mass fraction of AgNW in the freeze-dried solid samples), the average X-band SE_T increases more than 20 dB from 44 to 66 dB (Figure 3d). Herein, the SE_A increases extensively from ~35 to ~57 dB. The embedded high-conductive one-dimensional AgNW can effectively connect the dispersive MS fillers to optimize the conductive network. As a result, the cell walls with a higher conductivity could enhance the EMW loss capability of incident EMWs, improving the EMI SE of the hydrogels. More interestingly, the interactions between EMWs and cell walls were further amplified by the biomimetic aligned pore structure of the hydrogels.[7, 26] As for MS-based hydrogels, the EMI SE is measured when the propagation direction of the incident EMWs is parallel and perpendicular to the aligned pore channels, respectively.[5] For the MS-based hydrogels, the perpendicular EMI SE (pe-SE), corresponding to that when the propagation direction of the incident EMWs is perpendicular to the aligned pore channels, is ~44 dB and slightly higher than that of ~43 dB in the parallel direction (pa-SE). This is different from that an obvious anisotropy in EMI SE can be observed in the anisotropic porous foams/aerogels ever reported.[25-27] We assume that although the multiple reflections of incident EMWs in different propagation directions are different, the relatively low EMW absorption capability of cell walls cannot make a significant

difference in the SE_T of hydrogels without AgNW. This is also demonstrated by the low pe-SE and pa-SE values of the corresponding freeze-dried MS-based aerogels (Figure S11). However, the addition of low-content AgNW further promotes the pa-SE from 43 to 60 dB, which is significantly lower than that of the pe-SE of 66 dB (Figure 3e). Compared with pa-SE_A, the higher pe-SE_A further illustrates that the aligned cell walls can contribute to the multiple reflections of incident EMWs and thus significantly increasing the EMI SE for the hydrogels (Figure 3f). In short, the AgNW can increase the intrinsic conductivity and enhance the EMW dissipated capability of cell walls, which can be further amplified by the biomimetic ordered porous structure of the MS-based hydrogels. This leads to a good EMI shielding performance.

To better understand the high EMI shielding performance of MS-based hydrogels, the schematic diagram of EMI shielding is presented in Figure 3g. Thanks to the high electrical conductivity of MS, the increased mobile charge carriers and conductivity of the hydrogels result in the high reflection loss of incident EMWs.[49] Subsequently, the EMWs propagating into the aligned pore channels undergo multiple reflections or scatterings due to the abundant cell wall-pore interfaces, prolonging the propagation path of EMWs for more interactions with the cell walls owning high EMW loss capability. In the hydrogels, the synergistic efforts of multiple reflections, conductive loss, and polarization loss stemming from charge carriers of MS and AgNW, heterogeneous interfaces, and changed hydrogen bond networks associated with water molecules, result in the almost perfect consumption of the EMW energy. In addition, some defects and functional groups derived from MS can induce polarization loss, improving the EMI shielding performance. Particularly, the conductivity of cell walls further increases with the addition of AgNW, which led to the significant enhancement of multiple reflections induced EMW loss due to the

biomimetic aligned porous structure of the MS-based hydrogels. This leads to the distinct anisotropic EMI shielding performance of MS-based hydrogels, which has never been reported in previous work. This also contributes to the significant improvement of the EMI shielding performance of the MS-based hydrogels. In a word, combined with the simple, facile, and scalable preparation approach, we reuse the "trashed MXene" to fabricate the ultra-flexible and durable MS-based biomimetic ordered porous hydrogels with good EMI shielding performance.

Developing multifunctionalities is vital and a growing tendency for future EMI shielding materials. Since our MS-based hydrogels are highly flexible and robust, we briefly explore that they can be effortlessly attached to the human body as wearable sensors for detecting human motions.[50] The MS-based hydrogels with 60 wt% PVA are selected to construct the wearable sensors since they have a similar modulus to the soft tissues, such as muscles and tendons in the human body (**Figure 4**a). Upon stretching the hydrogels, the resistance is increased because of the elongated conductive path. The gauge factor (GF) corresponding to the sensitivity of the hydrogel sensors is also calculated (Figure 4b), which reveals a relatively high strain sensitivity. The resistance change of the sensor is reversible and repeatable, at the 12.5%, 30%, and 50% cyclic strains, showing reliable sensing performance. Imitating the bending of joints, when the hydrogel sensor is bent from the straightened state (0°) to 30°, 60°, and 90° and then held steady, respectively, the resistance increases accordingly due to the bending induced stretching and then remains constant. This exhibits the usefulness of our sensors in detecting various human motions from small to large strain activities. As the finger attached to the sensor bends and returns, the resistance of the hydrogel sensor increases sensitively and recovers periodically (Figure 4e–g). In addition, subtle motion such as tapping is well detected (Figure 4h). From this, the *Morse Code* can be edited and transmitted remotely by

tapping, and some numbers and words such as "*123*", "*MS*" and "*HYDROGEL*" are compiled (Figure 4i), respectively. These explorations further extend the application potentials of the MS-based hydrogels as flexible, multifunctional, high-performance next-generation electronics.

Conclusions

The MS-based hydrogels with biomimetic ordered pore structures are fabricated *via* scalable ice-templated freezing and salting-out treatments. The robust framework composed of highly crosslinked MS not only stabilizes the aligned micrometer-sized pore structure but also contributes to the formation of high-strength hydrogels with mechanical ultra-flexibility, including bendability and even stretchability. Upon the synergistic effects of the MS-based conductive network,[30] PVA chains, water, and porous structure, the MS-based hydrogels exhibit good EMI shielding performance. Our MS-based hydrogels possess the EMI SE of 31 to 91 dB at a thickness of 1.0 to 7.5 mm, respectively, and an SE of more than 40 dB at a thickness of 2.0 mm in the ultra-broadband GHz band (8.2–40 GHz). Particularly, we quantitatively identify the influences of water of hydrogels on EMI shielding performance *via* a resumable approach to control the water fraction. Moreover, with the addition of AgNWs, the shielding performance of the MS-based hydrogels significantly increases, which is derived from the enhanced multiple reflections loss caused by the biomimetic aligned porous structure. This contributes to the implementation of an anisotropic EMI shielding performance for the hydrogel-based EMI shields, achieving the preparation of hydrogel with controllable EMI shielding performance derived from interior porous structure beyond the material constituent. This also leads to significantly improved EMI shielding performance of the MS-based hydrogels, which outperform other EMI shielding materials ever reported. In addition, the MS-based

hydrogels show sensitive and reliable detections of human motions and smart coding as wearable flexible devices. The preparation of the MS-based hydrogels based on the "MXene trash" is waste-free, scalable, and low-cost. Combined with the multifunctional, outstanding EMI shielding performance, the high-strength, ultra-flexible MS-based hydrogels suggest promising application potentials for next-generation electronics.

Experimental

Preparation of the MS and MS-based hydrogels. The etching of the Ti_3AlC_2 MAX phase (Laizhou Kai Kai Ceramic Materials Co., Ltd.) was performed using the minimally intensive layer delamination or "MILD" synthesis route as shown in our previous work. Typically, 0.5 g lithium fluoride was dissolved in a 20 mL 4.5 M hydrochloric acid solution. Afterward, 0.5 g Ti_3AlC_2 MAX was added to the aforementioned mixture and incubated at 35°C for 24 h. After the reaction, the suspension was centrifuged at 3500 rpm and redispersed with deionized water until the pH was up to 6. Subsequently, the suspension was shaken for 20 min and centrifuged at 3500 rpm for 5 min. After decanting the supernatant, the MS that was generally trashed was left at the bottom of the centrifuge tube. A certain amount of PVA (PVA-124, the average degree of polymerization of 2, 400 to 2, 500, 98%–99% hydrolyzed) aqueous solution and MS were mixed to form a series of homogeneous mixtures with various MS contents, and the Table S3 enumerated the details of the mixtures. The concentration of PVA in the homogeneous mixture was 4 wt%. Subsequently, the homogeneous mixture was poured into a container made of polytetrafluoroethylene (PTFE) and a metallic bottom as a cold finger immersed in the liquid nitrogen for directional freezing. The frozen samples were then immersed into a 4.0 M sodium chloride solution for crosslinking of 24 h. After

soaking the hydrogel samples in DI water to remove the ions, the MS-based hydrogels with aligned micrometer-sized pores were fabricated. The MS-based hydrogels containing a small fraction of AgNWs were prepared *via* the same procedure with an extra addition of AgNWs (an average length of 100–200 μm and an average diameter of 50 nm, Nanjing XFNANO Materials Tech Co., Ltd) in a mixture of MS and PVA. To figure out the effects of water on EMI shielding, the MS-based hydrogels were freeze-dried with different time to acquire a series of hydrogels with different water contents.

Characterization. For characterization of the pore morphology and microstructure of the hydrogels, all hydrogel samples were freeze-dried using a freeze-dryer (SCIENTZ-12N). Scanning electron microscopy (SEM, Hitachi SU-70) and transmission electron microscopy (TEM, JEOL JEM-2100) were employed to characterize the morphology and microstructure. The phase information and surface chemical states were investigated using an X-ray diffractometer (XRD, Cu K_{α}, DMAX-2500PC, Rigaku). The mechanical performance of the MS-based hydrogels was carried out by IS-200N and at least five samples were tested for each component of samples. Unless special mentioned, the tensile direction was parallel to the oriented channel direction. The resistances were measured in a four-probe method by the Tonghui test system (TH26011CS) to calculate the electrical conductivity (δ). The hydrogels with aligned pores showed similar electrical conductivity due to the interconnected conductive cell walls in different directions. EMI SE values and electromagnetic parameters in the frequency range of 8.2–40.0 GHz were measured by a vector network analyzer (VNA, Agilent PNA N5244A) in the waveguide method. Unless special mentioned, the EMI SE was measured when the propagation direction of the incident EMWs was perpendicular to the aligned pore channels. More than three specimens were tested for each component. The size of the

tested samples was cut into 22.86 mm × 10.16 mm (length × width) in the tested frequency range of 8.2–12.4 GHz (X-band), 15.74 mm × 7.87 mm (length × width) in the tested frequency range of 12.4–18 GHz (Ku-band), 10.67 mm × 5.33 mm (length × width) in the tested frequency range of 18–26.5 GHz (K-band), and 7.12 mm × 3.56 mm (length × width) in the tested frequency range of 26.5–40 GHz (Ka-band). The S-parameters were recorded and used to calculate the SE_T, SE_R, and SE_A, power coefficient of *A*, *R*, and *T* based on the following formulas:

$$R = |S_{11}|^2 = |S_{22}|^2 \quad (1)$$

$$T = |S_{12}|^2 = |S_{21}|^2 \quad (2)$$

$$A = 1 - R - T \quad (3)$$

$$SE_T\,(\mathrm{dB}) = 10\log\left(\frac{1}{T}\right) \quad (4)$$

$$SE_R\,(\mathrm{dB}) = -10\log\left(1 - {S_{11}}^2\right) = -10\log\left(1 - {S_{22}}^2\right) \quad (5)$$

$$SE_A\,(\mathrm{dB}) = SE_T - SE_R \quad (6)$$

Supporting Information

Supporting Information is available free of charge. SEM image of Ti_3AlC_2 MAX; Basic characterization of $Ti_3C_2T_x$ MXene nanosheets; XRD patterns, SEM, EDS, and TEM images of MS-based samples; supplementary mechanical properties and EMI SE of samples; the stability curve of conductivity of hydrogel; the SEM images, XRD patterns, and EDS mappings of Ag NWs and corresponding hydrogels; the supplementary EMI SE of the freeze-dried hydrogels; comparison of modulus and EMI shielding performance of MS-based hydrogels.

Acknowledgments

This work was supported by the National Key R&D Program of China (No. 2021YFB3502500), Natural Science Foundation of Shandong Province (No. 2022HYYQ-014, ZR2016BM16), and the Provincial Key Research and Development Program of Shandong (No. 2019JZZY010312, 2021ZLGX01), "20 Clauses about Colleges and Universities (new)" (Independent Training of Innovation Team) Program (2021GXRC036), Shenzhen municipal special fund for guiding local scientific and Technological Development (China 2021Szvup071), and Qilu Young Scholar Program of Shandong University (No. 31370082163127).

References:

(1) Wan, S.; Li, X.; Chen, Y.; Liu, N.; Du, Y.; Dou, S.; Jiang, L.; Cheng, Q. High-strength Scalable MXene Films through Bridging-induced Densification. *Science* **2021**, *374* (6563), 96-99. DOI: 10.1126/science.abg2026.

(2) Iqbal, A.; Shahzad, F.; Hantanasirisakul, K.; Kim, M.-K.; Kwon, J.; Hong, J.; Kim, H.; Kim, D.; Gogotsi, Y.; Koo, C. M. Anomalous Absorption of Electromagnetic Waves by 2D Transition Metal Carbonitride Ti_3CNT_x (MXene). *Science* **2020**, *369* (6502), 446-450. DOI: 10.1126/science.aba7977.

(3) Sun, R.; Zhang, H.-B.; Liu, J.; Xie, X.; Yang, R.; Li, Y.; Hong, S.; Yu, Z.-Z. Highly Conductive Transition Metal Carbide/Carbonitride(MXene)@polystyrene Nanocomposites Fabricated by Electrostatic Assembly for Highly Efficient Electromagnetic Interference Shielding. *Adv. Funct. Mater.* **2017**, *27* (45), 1702807. DOI: 10.1002/adfm.201702807.

(4) Chen, Z.; Xu, C.; Ma, C.; Ren, W.; Cheng, H.-M. Lightweight and Flexible Graphene Foam Composites for High-Performance Electromagnetic Interference Shielding. *Adv. Mater.* **2013**, *25* (9), 1296-1300. DOI: 10.1002/adma.201204196.

(5) Zeng, Z.; Jin, H.; Chen, M.; Li, W.; Zhou, L.; Xue, X.; Zhang, Z. Microstructure Design of Lightweight, Flexible, and High Electromagnetic Shielding Porous Multiwalled Carbon Nanotube/Polymer Composites. *Small* **2017**, *13* (34), 1701388. DOI: 10.1002/smll.201701388.

(6) Wu, N.; Zeng, Z.; Kummer, N.; Han, D.; Zenobi, R.; Nyström, G. Ultrafine Cellulose Nanofiber-Assisted Physical and Chemical Cross-Linking of MXene Sheets for Electromagnetic Interference Shielding. *Small Methods* **2021**, *5* (12), 2100889. DOI: 10.1002/smtd.202100889.

(7) Zeng, Z.; Jin, H.; Chen, M.; Li, W.; Zhou, L.; Zhang, Z. Lightweight and Anisotropic Porous MWCNT/WPU Composites for Ultrahigh Performance Electromagnetic Interference Shielding. *Adv.*

Funct. Mater. **2016**, *26* (2), 303-310. DOI: 10.1002/adfm.201503579.

(8) Zeng, Z.-H.; Wu, N.; Wei, J.-J.; Yang, Y.-F.; Wu, T.-T.; Li, B.; Hauser, S. B.; Yang, W.-D.; Liu, J.-R.; Zhao, S.-Y. Porous and Ultra-Flexible Crosslinked MXene/Polyimide Composites for Multifunctional Electromagnetic Interference Shielding. *Nano-Micro Lett.* **2022**, *14* (1), 59. DOI: 10.1007/s40820-022-00800-0.

(9) Zhao, S.; Zhang, H.-B.; Luo, J.-Q.; Wang, Q.-W.; Xu, B.; Hong, S.; Yu, Z.-Z. Highly Electrically Conductive Three-Dimensional $Ti_3C_2T_x$ MXene/Reduced Graphene Oxide Hybrid Aerogels with Excellent Electromagnetic Interference Shielding Performances. *ACS Nano* **2018**, *12* (11), 11193-11202. DOI: 10.1021/acsnano.8b05739.

(10) Liu, J.; Zhang, H.-B.; Sun, R.; Liu, Y.; Liu, Z.; Zhou, A.; Yu, Z.-Z. Hydrophobic, Flexible, and Lightweight MXene Foams for High-Performance Electromagnetic-Interference Shielding. *Adv. Mater.* **2017**, *29* (38), 1702367. DOI: 10.1002/adma.201702367.

(11) Xie, Y.; Liu, S.; Huang, K.; Chen, B.; Shi, P.; Chen, Z.; Liu, B.; Liu, K.; Wu, Z.; Chen, K.; et al. Ultra-broadband Strong Electromagnetic Interference Shielding with Ferromagnetic Graphene Quartz Fabric. *Adv. Mater.* **2022**, Accepted Author Manuscript 22029822202982. DOI: 10.1002/adma.202202982.

(12) Hua, M.; Wu, S.; Ma, Y.; Zhao, Y.; Chen, Z.; Frenkel, I.; Strzalka, J.; Zhou, H.; Zhu, X.; He, X. Strong Tough Hydrogels via the Synergy of Freeze-casting and Salting out. *Nature* **2021**, *590* (7847), 594-599. DOI: 10.1038/s41586-021-03212-z.

(13) Zhang, Y. S.; Khademhosseini, A. Advances in Engineering Hydrogels. *Science* **2017**, *356* (6337), eaaf3627. DOI: doi:10.1126/science.aaf3627.

(14) Wu, S.; Hua, M.; Alsaid, Y.; Du, Y.; Ma, Y.; Zhao, Y.; Lo, C.-Y.; Wang, C.; Wu, D.; Yao, B.;

et al. Poly(vinyl alcohol) Hydrogels with Broad-Range Tunable Mechanical Properties via the Hofmeister Effect. *Adv. Mater.* **2021**, *33* (11), 2007829. DOI: 10.1002/adma.202007829.

(15) Wang, C.; Liu, Y.; Qu, X.; Shi, B.; Zheng, Q.; Lin, X.; Chao, S.; Wang, C.; Zhou, J.; Sun, Y.; et al. Ultra-Stretchable and Fast Self-Healing Ionic Hydrogel in Cryogenic Environments for Artificial Nerve Fiber. *Adv. Mater.* **2022**, *34* (16), 2105416. DOI: 10.1002/adma.202105416.

(16) Andryieuski, A.; Kuznetsova, S. M.; Zhukovsky, S. V.; Kivshar, Y. S.; Lavrinenko, A. V. Water: Promising Opportunities for Tunable All-dielectric Electromagnetic Metamaterials. *Sci. Rep.* **2015**, *5* (1), 13535. DOI: 10.1038/srep13535.

(17) Buchner, R.; Barthel, J.; Stauber, J. The Dielectric Relaxation of Water between 0°C and 35°C. *Chem. Phys. Lett.* **1999**, *306* (1), 57-63. DOI: 10.1016/S0009-2614(99)00455-8.

(18) Meissner, T.; Wentz, F. J. The Complex Dielectric Constant of Pure and Sea Water from Microwave Satellite Observations. *IEEE T. Geosci. Remote* **2004**, *42* (9), 1836-1849. DOI: 10.1109/TGRS.2004.831888.

(19) Iqbal, A.; Sambyal, P.; Koo, C. M. 2D MXenes for Electromagnetic Shielding: A Review. *Adv. Funct. Mater.* **2020**, *30* (47), 2000883. DOI: 10.1002/adfm.202000883.

(20) Thomassin, J.-M.; Jerome, C.; Pardoen, T.; Bailly, C.; Huynen, I.; Detrembleur, C. Polymer/carbon Based Composites as Electromagnetic Interference (EMI) Shielding Materials. *Mat. Sci. Eng. R* **2013**, *74* (7), 211-232. DOI: 10.1016/j.mser.2013.06.001.

(21) Lai, D.; Chen, X.; Wang, G.; Xu, X.; Wang, Y. Arbitrarily Reshaping and Instantaneously Self-Healing Graphene Composite Hydrogel with Molecule Polarization-enhanced ultrahigh Electromagnetic Interference Shielding Performance. *Carbon* **2022**, *188*, 513-522. DOI: 10.1016/j.carbon.2021.12.047.

(22) Liu, J.; Mckeon, L.; Garcia, J.; Pinilla, S.; Barwich, S.; Möbius, M.; Stamenov, P.; Coleman, J. N.; Nicolosi, V. Additive Manufacturing of Ti_3C_2-MXene-Functionalized Conductive Polymer Hydrogels for Electromagnetic-Interference Shielding. *Adv. Mater.* **2022**, *34* (5), 2106253. DOI: 10.1002/adma.202106253.

(23) Fu, F.; Wang, J.; Zeng, H.; Yu, J. Functional Conductive Hydrogels for Bioelectronics. *ACS Mater. Lett.* **2020**, *2* (10), 1287-1301. DOI: 10.1021/acsmaterialslett.0c00309.

(24) Wang, J.; Li, Q.; Li, K.; Sun, X.; Wang, Y.; Zhuang, T.; Yan, J.; Wang, H. Ultra-High Electrical Conductivity in Filler-free Polymeric Hydrogels toward Thermoelectrics and Electromagnetic Interference Shielding. *Adv. Mater.* **2022***, 34* (12), 2109904. DOI: 10.1002/adma.202109904.

(25) Zeng, Z.; Wang, C.; Siqueira, G.; Han, D.; Huch, A.; Abdolhosseinzadeh, S.; Heier, J.; Nüesch, F.; Zhang, C.; Nyström, G. Nanocellulose-MXene Biomimetic Aerogels with Orientation-Tunable Electromagnetic Interference Shielding Performance. *Adv. Sci.* **2020**, *7* (15), 2000979. DOI: 10.1002/advs.202000979.

(26) Zeng, Z.; Wu, T.; Han, D.; Ren, Q.; Siqueira, G.; Nyström, G. Ultralight, Flexible, and Biomimetic Nanocellulose/Silver Nanowire Aerogels for Electromagnetic Interference Shielding. *ACS Nano* **2020**, *14* (3), 2927-2938. DOI: 10.1021/acsnano.9b07452.

(27) Zeng, Z.; Jin, H.; Chen, M.; Li, W.; Zhou, L.; Xue, X.; Zhang, Z. Microstructure Design of Lightweight, Flexible, and High Electromagnetic Shielding Porous Multiwalled Carbon Nanotube/Polymer Composites. *Small* **2017**, *13* (34). DOI: 10.1002/smll.201701388.

(28) Abdolhosseinzadeh, S.; Schneider, R.; Verma, A.; Heier, J.; Nüesch, F.; Zhang, C. Turning Trash into Treasure: Additive Free MXene Sediment Inks for Screen-Printed Micro-Supercapacitors. *Adv. Mater.* **2020**, *32* (17), 2000716. DOI: 10.1002/adma.202000716.

(29) Hu, M.; Zhang, H.; Hu, T.; Fan, B.; Wang, X.; Li, Z. Emerging 2D MXenes for Supercapacitors: Status, Challenges and Prospects. *Chem. Soc. Rev.* **2020**, *49* (18), 6666-669. DOI: 10.1039/D0CS00175A.

(30) Lin, Z.; Liu, J.; Peng, W.; Zhu, Y.; Zhao, Y.; Jiang, K.; Peng, M.; Tan, Y. Highly Stable 3D $Ti_3C_2T_x$ MXene-based Foam Architectures toward High-Performance Terahertz Radiation Shielding. *ACS Nano* **2020**, *14* (2), 2109-2117. DOI: 10.1021/acsnano.9b08832.

(31) Shi, S.; Qian, B.; Wu, X.; Sun, H.; Wang, H.; Zhang, H.-B.; Yu, Z.-Z.; Russell, T. P. Self-Assembly of MXene-Surfactants at Liquid–liquid Interfaces: From Structured Liquids to 3D Aerogels. *Angew. Chem. Int. Ed.* **2019**, *58* (50), 18171-18176. DOI: 10.1002/anie.201908402.

(32) Xu, H.; Yin, X.; Li, X.; Li, M.; Liang, S.; Zhang, L.; Cheng, L. Lightweight Ti_2CT_x MXene/Poly(vinyl alcohol) Composite Foams for Electromagnetic Wave Shielding with Absorption-dominated Feature. *ACS Appl. Mater. Interfaces* **2019**, *11* (10), 10198-10207. DOI: 10.1021/acsami.8b21671.

(33) Zhang, Y.-Z.; El-Demellawi, J. K.; Jiang, Q.; Ge, G.; Liang, H.; Lee, K.; Dong, X.; Alshareef, H. N. MXene Hydrogels: Fundamentals and Applications. *Chem. Soc. Rev.* **2020**, *49* (20), 7229-7251, 10.1039/D0CS00022A. DOI: 10.1039/D0CS00022A.

(34) Ling, Z.; Ren, C. E.; Zhao, M.-Q.; Yang, J.; Giammarco, J. M.; Qiu, J.; Barsoum, M. W.; Gogotsi, Y. Flexible and Conductive MXene Films and Nanocomposites with High Capacitance. *P. Natl. Acad. Sci. USA* **2014**, *111* (47), 16676. DOI: 10.1073/pnas.1414215111.

(35) Zhang, S.; Ying, H.; Huang, P.; Yang, T.; Han, W.-Q. Hierarchical Utilization of raw $Ti_3C_2T_x$ MXene for Fast Preparation of Various $Ti_3C_2T_x$ MXene Derivatives. *Nano Res.* **2022**, *15* (3), 2746-2755. DOI: 10.1007/s12274-021-3847-4.

(36) Xu, H.; Zhu, W.; Sun, F.; Qi, H.; Zou, J.; Laine, R.; Ding, W. Turning Trash into Treasure: MXene with Intrinsic LiF Solid Electrolyte Interfaces Performs Better and Better during Battery Cycling. *Adv. Mater. Technol-US* **2021**, *6* (3), 2000882. DOI: 10.1002/admt.202000882.

(37) Sano, K.; Ishida, Y.; Aida, T. Synthesis of Anisotropic Hydrogels and Their Applications. *Angew. Chem. Int. Ed.* **2018**, *57* (10), 2532-2543. DOI: 10.1002/anie.201708196.

(38) Jaspers, M.; Rowan, A. E.; Kouwer, P. H. J. Tuning Hydrogel Mechanics Using the Hofmeister Effect. *Adv. Funct. Mater.* **2015**, *25* (41), 6503-6510. DOI: 10.1002/adfm.201502241.

(39) Wang, X.; Qiao, C.; Jiang, S.; Liu, L.; Yao, J. Strengthening Gelatin Hydrogels using the Hofmeister Effect. *Soft Matter* **2021**, *17* (6), 1558-1565. DOI: 10.1039/D0SM01923B.

(40) Zhang, H.-B.; Yan, Q.; Zheng, W.-G.; He, Z.; Yu, Z.-Z. Tough Graphene-polymer Microcellular Foams for Electromagnetic Interference Shielding. *ACS Appl. Mater. Interfaces* **2011**, *3* (3), 918-924. DOI: 10.1021/am200021v.

(41) Yan, D. X.; Pang, H.; Li, B.; Vajtai, R.; Xu, L.; Ren, P. G.; Wang, J. H.; Li, Z. M. Structured Reduced Graphene Oxide/polymer Composites for Ultra-efficient Electromagnetic Interference Shielding. *Adv. Funct. Mater.* **2015**, *25* (4), 559-566. DOI: 10.1039/c9ra04244j.

(42) Al-Saleh, M. H.; Saadeh, W. H.; Sundararaj, U. EMI Shielding Effectiveness of Carbon Based Nanostructured Polymeric Materials: A Comparative Study. *Carbon* **2013**, *60*, 146-156. DOI: 10.1016/j.carbon.2013.04.008.

(43) Liu, X.; Li, Y.; Sun, X.; Tang, W.; Deng, G.; Liu, Y.; Song, Z.; Yu, Y.; Yu, R.; Dai, L.; et al. Off/on Switchable Smart Electromagnetic Interference Shielding Aerogel. *Matter* **2021**, *4* (5), 1735-1747. DOI: 10.1016/j.matt.2021.02.022.

(44) Chen, Y.; Yang, Y.; Xiong, Y.; Zhang, L.; Xu, W.; Duan, G.; Mei, C.; Jiang, S.; Rui, Z.; Zhang,

K. Porous Aerogel and Sponge Composites: Assisted by Novel Nanomaterials for Electromagnetic Interference Shielding. *Nano Today* **2021**, *38*, 101204. DOI: 10.1016/j.nantod.2021.101204.

(45) Du, Y.; Xu, J.; Fang, J.; Zhang, Y.; Liu, X.; Zuo, P.; Zhuang, Q. Ultralight, Highly Compressible, Thermally Stable MXene/aramid Nanofiber Anisotropic Aerogels for Electromagnetic Interference Shielding. *J. Mater. Chem. A* **2022**, *10* (12), 6690-6700. DOI: 10.1039/D1TA11025J.

(46) Xu, J.; Li, R.; Ji, S.; Zhao, B.; Cui, T.; Tan, X.; Gou, G.; Jian, J.; Xu, H.; Qiao, Y.; et al. Multifunctional Graphene Microstructures Inspired by Honeycomb for Ultrahigh Performance Electromagnetic Interference Shielding and Wearable Applications. *ACS Nano* **2021**, *15* (5), 8907-8918. DOI: 10.1021/acsnano.1c01552.

(47) Zeng, Z.; Wang, C.; Wu, T.; Han, D.; Luković, M.; Pan, F.; Siqueira, G.; Nyström, G. Nanocellulose Assisted Preparation of Ambient Dried, Large-scale and Mechanically Robust Carbon Nanotube Foams for Electromagnetic Interference Shielding. *J. Mater. Chem. A* **2020**, *8* (35), 17969-17979. DOI: 10.1039/D0TA05961G.

(48) Song, W.-L.; Zhang, Y.-J.; Zhang, K.-L.; Wang, K.; Zhang, L.; Chen, L.-L.; Huang, Y.; Chen, M.; Lei, H.; Chen, H.; et al. Ionic Conductive Gels for Optically Manipulatable Microwave Stealth Structures. *Adv. Sci.* **2020**, *7* (2), 1902162. DOI: 10.1002/advs.201902162.

(49) Sun, Z. M. Progress in Research and Development on MAX Phases: A Family of Layered Ternary Compounds. *Int. Mater. Rev.* **2011**, *56* (3), 143-166. DOI: 10.1179/1743280410Y.0000000001.

(50) Liu, J.; Zheng, H.; Poh, P. S. P.; Machens, H.-G.; Schilling, A. F. Hydrogels for Engineering of Perfusable Vascular Networks. *Int. J. Mol. Sci.* **2015**, *16* (7), 15997-16016. DOI:

10.3390/ijms160715997

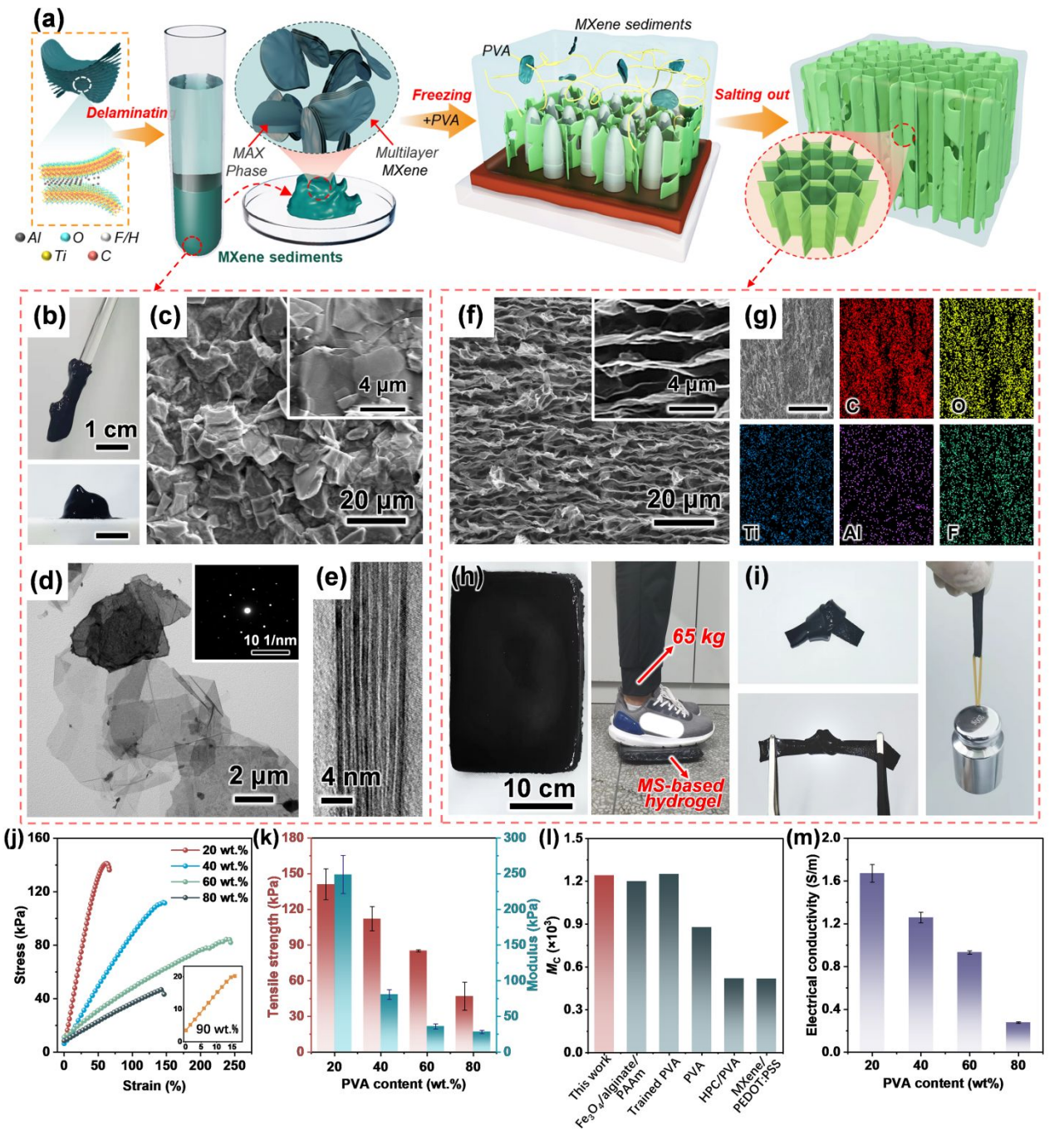

Figure 1. (a) Schematic showing the preparation process of the MS-based hydrogels. (b) Photos of as-prepared MS (top) and that strands for 1 hour (bottom), showing a highly viscous nature. (c) SEM image of the MS particles. (d) TEM (inset shows electron diffraction image) image of the MS, including (e) un-exfoliated m-MXene. (f) SEM image of MS-based hydrogels (parallel to pore channel) and (g) the element mappings of C, O, Ti, Al, and F. (h) Large-area MS-based hydrogel that is larger than an A4 paper (around 21×30 cm^2) and a photo of the hydrogel that sustains a person

weighing 65 kg. (i) Photographs of the ultra-flexible MS-based hydrogels with bending, twisting, and stretching capability (left), and an MS-based hydrogel stripe (~1 g) holding up a load of 200 g (right), (j) Tensile stress-strain curves, (k) tensile strength and Youngs's modulus, (l) the comparison of M_S with other typical hydrogels, and (m) electrical conductivity of the MS-based hydrogels with various PVA contents.

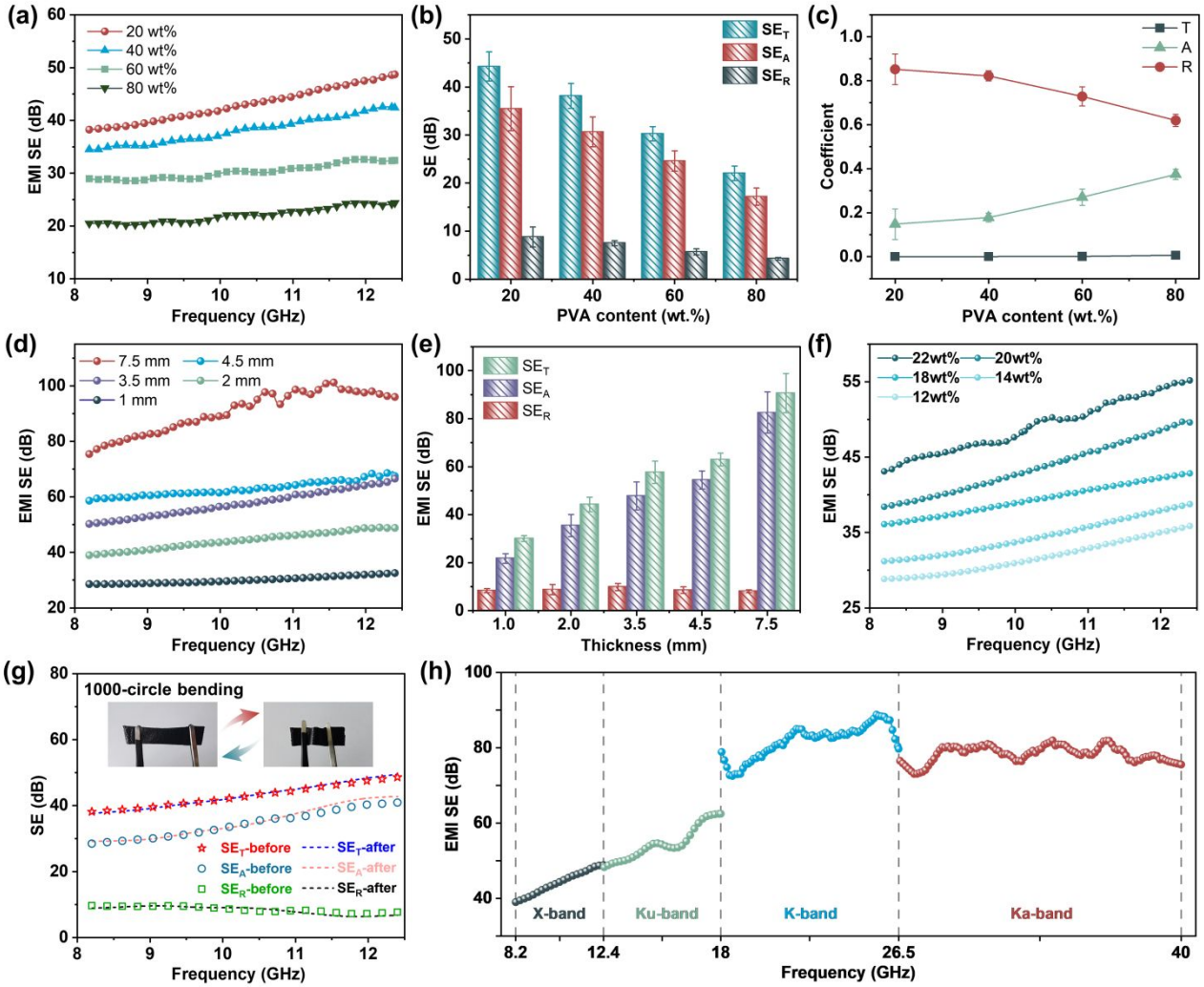

Figure 2. (a) The X-band EMI SE, (b) SE_R, SE_A, and SE_T, (c) power coefficients of the hydrogels with various PVA contents. (d) EMI SE and (e) SE_R, SE_A, and SE_T of various thicknesses of MS-based (20 wt% PVA) hydrogels. (f) Effects of solid content (the mass fraction of MS and PVA) on the EMI SE of MS-based hydrogels (20 wt% PVA). (g) The X-band EMI SE of MS-based hydrogels (20 wt% PVA) before and after 1000 cycles of bending. (h) The EMI SE in the ultra-broadband GHz frequency ranges including X, Ku, K, and Ka bands.

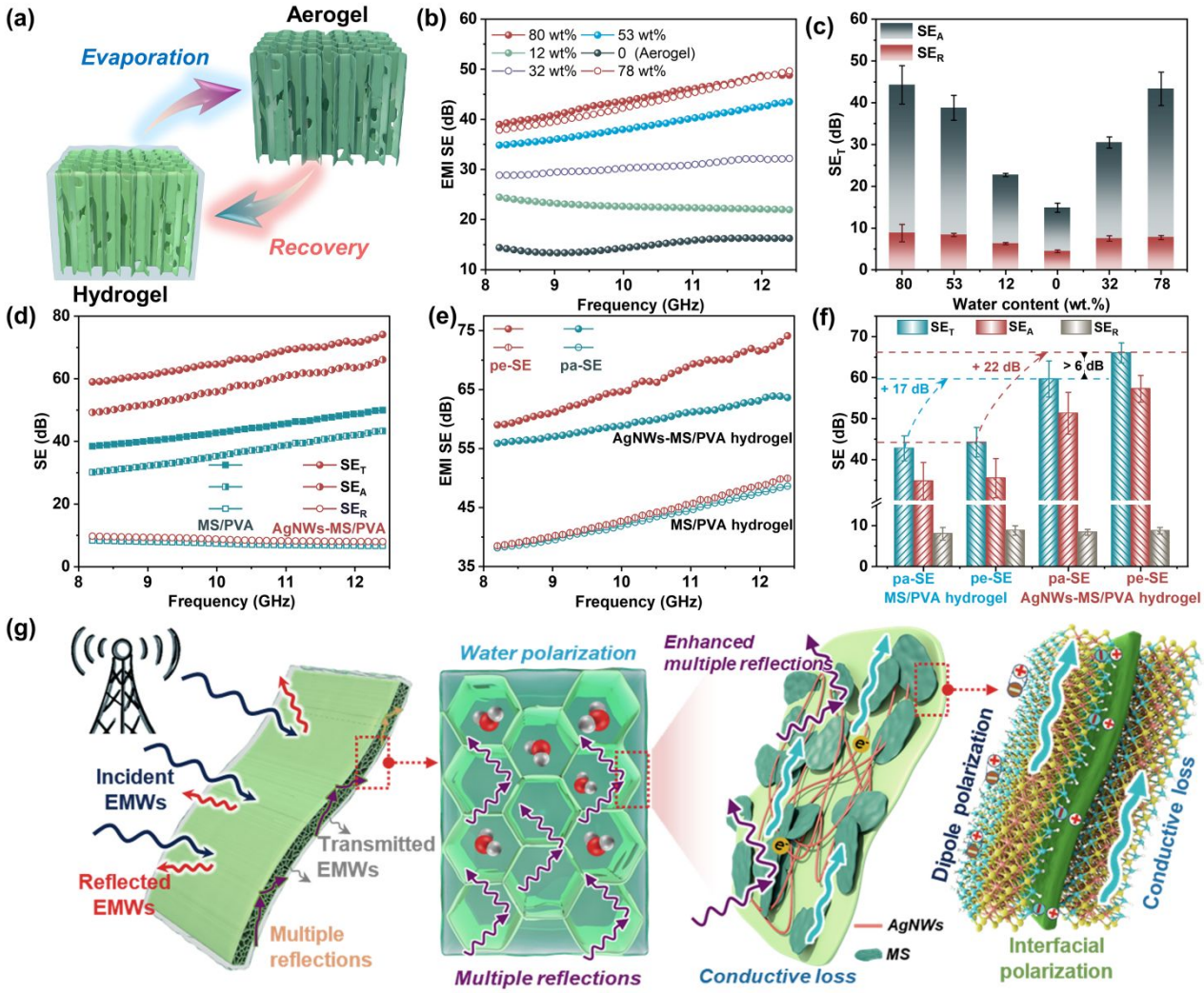

Figure 3. (a) The schematic showing the reversible conversion between hydrogel and aerogel. (b) The EMI SE and (c) SE_A, SE_R, and SE_T values of MS-based hydrogels with various water contents. (d) The SE_A, SE_R, and SE_T values of the MS-based and AgNWs-MS-based hydrogels (~20 wt% PVA). (e) The EMI SE, and (f) SE_A, SE_R, and SE_T of the MS-based and AgNWs-MS-based hydrogels (~20 wt% PVA) in different directions. (g) The EMI shielding mechanism of the hydrogels with biomimetic ordered porous structure.

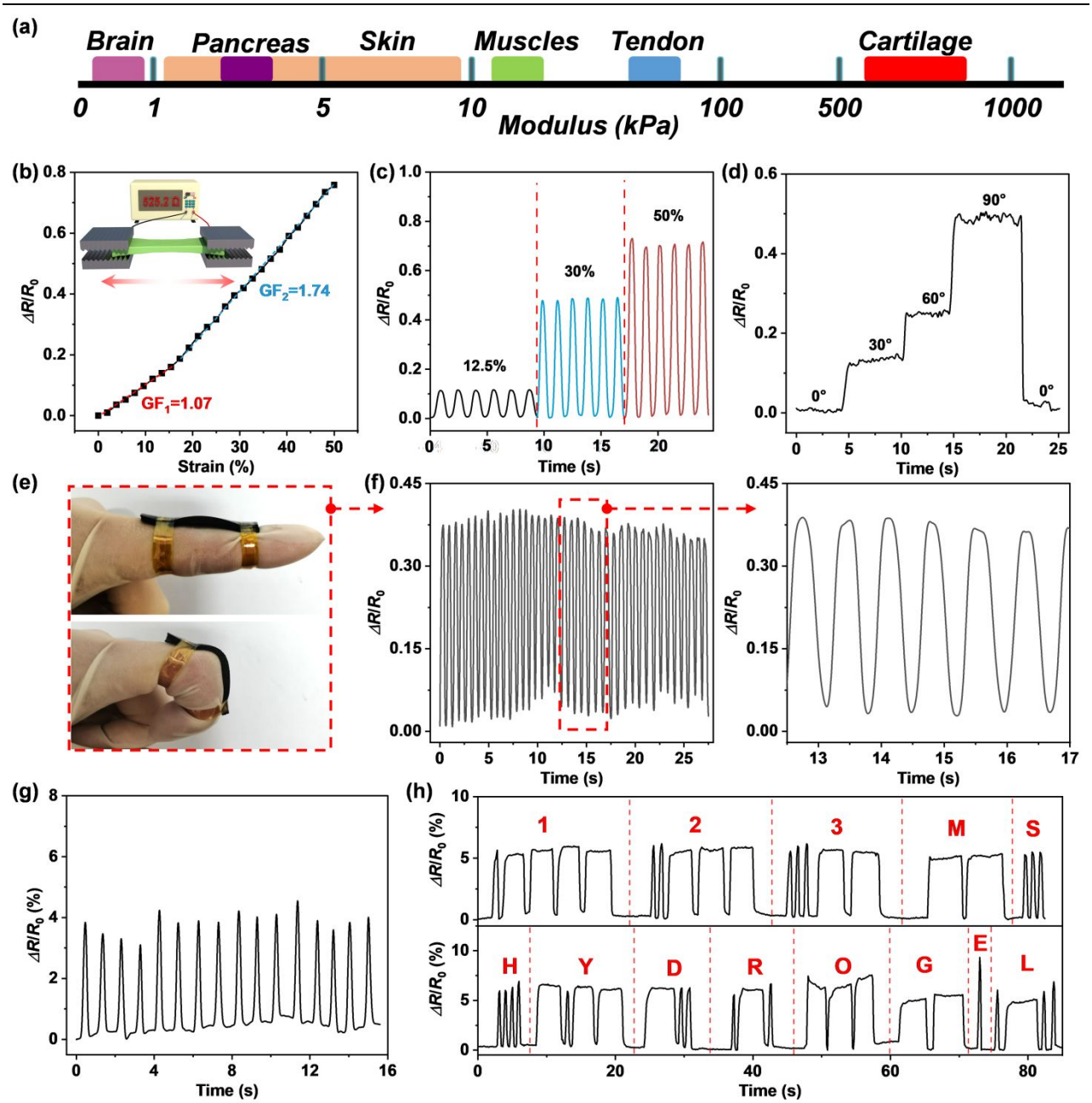

Figure 4. (a) Young's modulus of natural soft tissues. (b) The resistance changes and strain GF of MS-based hydrogels. (c) Relatively resistance change of MS-based hydrogels under different tensile strains. Resistance changes of the sensor in response to different mechanical signals: (e) bending-induced stretch with various angles, (e, f) finger bending, and (g) fast clicking. Through the relative resistance change signals responding to the decoding of (h) "*123*", "*MS*", and "*HYDROGEL*".

Table of Contents